1995ApJ...441..603B

THE ASTROPHYSICAL JOURNAL, 441:603–616, 1995 March 10
© 1995. The American Astronomical Society. All rights reserved. Printed in U.S.A.

A COMPARISON OF NEAR-INFRARED SPECTRA OF THE GALACTIC CENTER COMPACT He I EMISSION-LINE SOURCES AND EARLY-TYPE MASS-LOSING STARS

R. D. BLUM,[1] D. L. DEPOY,[1] AND K. SELLGREN[1,2]
Astronomy Department, Ohio State University, 174 W. 18th Avenue, Columbus, OH 43210
Received 1994 July 8; accepted 1994 September 22

ABSTRACT

We present $R \approx 570$ resolution K band spectra of eight sources in the Galactic center, including four sources within the IRS 16 cluster, IRS 13, IRS 1 W, and the compact He I emission-line sources AF (also known as AHH) and AHH NW. We also present $R \approx 570$ H and K band spectra of the AF source and nine galactic and LMC early-type mass-losing stars, including Ofpe/WN9, WN, and LBV stars. The spectra of both the Galactic center sources and the comparison stars show a wide range of behavior in the He I (1.70 μm, 2.06 μm, 2.11 μm) and H I (Brackett series) lines. While the Galactic center and comparison star spectra show some morphological similarities, we find significantly larger He I equivalent widths in the AF source and two galactic early-type mass-losing stars than in any of the LMC stars. Several of the Galactic center He I sources are found to have higher He I velocity widths than any of the galactic or LMC early-type mass-losing stars. At least one source, IRS 13, shows significant emission to the red of the He I 2.06 μm line emission, which may be a red wing to this line or a blend of other unidentified lines.

We also rule the Galactic center He I sources being normal OB giant/supergiants, WC, or WN7–8 stars based on a comparison of our spectra to published spectra of these types. We estimate the $BC_K = M_{bol} - M_K$ for the Galactic center sources as a function of effective temperature from published data on LBV, WN9, and Ofpe/WN9 stars, and use limits on the effective temperature to place the Galactic center sources in the H-R diagram.

Subject headings: Galaxy: center — infrared: ISM: lines and bands — Magellanic Clouds — stars: early-type — stars: mass loss

1. INTRODUCTION

What is the source of radiation that ionizes the gas and powers the dust emission at the Galactic center? Two models are debated: (1) accretion onto a massive black hole and (2) young ($\lesssim 10^7$ yr) massive stars. Genzel & Townes (1987) and Genzel, Hollenbach, & Townes (1994) present extensive reviews. Lebofsky, Rieke, & Tokunaga (1982) identified M supergiant stars in the Galactic center (GC), supporting the recent star formation model. More recently, Forrest et al. (1987), Allen, Hyland, & Hillier (1990), and Krabbe et al. (1991) have identified compact He I sources and/or Brα emission sources with no radio counterparts in the GC. Allen et al. (1990) and Krabbe et al. (1991) interpreted the He I and accompanying H I emission as arising in the extended mass-losing envelopes of hot, massive post–main-sequence stars. This interpretation is based on the similarity of the K band ($\lambda \approx 2.2$ μm) spectrum of the most prominent GC He I source (known as the AF star or the AHH star) and the relative He I to Brγ line measurements of other GC He I sources compared to similar spectra of optically classified stars in the Large Magellanic Cloud. In particular, the AF source has been classified as an Ofpe/WN9 star based on its K band spectrum as compared to similar spectra of a number of optically classified LMC stars with this classification (Allen et al. 1990). If correct, this interpretation provides the most substantial evidence to date for the star formation model.

Two alternate models for the IRS 16 sources have been proposed. Morris (1993) proposed these sources formed by collisions between stellar remnants and late-type stars. Tamblyn & Rieke (1993) interpret the IRS 16 sources as young stars but cooler F or G supergiants, as opposed to the hotter post–main-sequence stars discussed above. The He I emission would then arise in gas which is in close proximity to the IRS 16 sources (i.e., the winds from cool stars which are ionized by external sources).

Optical classification of the GC sources is impossible due to the large extinction from interstellar dust along the line of sight. It is therefore important to acquire as wide a range of spectroscopic and broad-band measurements as possible at longer wavelengths in order to understand the underlying physics of the GC He I sources. In this paper, we compare near-infrared (NIR) spectra of the GC He I sources with those of the early-type mass-losing stars in the LMC and representatives from the Galaxy. We present H ($\lambda \approx 1.65$ μm) and K spectra of the AF source, seven other GC He I sources (K band only) and nine early-type emission-line stars from the Galaxy and LMC. The LMC stars include five of those observed by McGregor, Hillier, & Hyland (1988; hereafter MHH); here we extend these spectra to the H band and include the LMC luminous blue variable (LBV) S Dor. The galactic sources include two Ofpe/WN9 stars (WR 85a and WR 122; van der Hucht et al. 1988) and the only galactic WN9 star (WR 108) which have no previously published NIR spectra. Periodic observation of these sources is important; we find large variations in the K band spectrum of at least one of the Ofpe/WN9 stars observed by MHH.

In what follows, we briefly review the Ofpe/WN9 class, make direct comparisons between the observed spectra of these stars

[1] Visiting Astronomer, Cerro Tololo Inter-American Observatory, National Optical Astronomy Observatories, which are operated by the Association of Universities for Research in Astronomy, Inc., under cooperative agreement with the National Science Foundation.
[2] Alfred P. Sloan Research Fellow.

© American Astronomical Society • Provided by the NASA Astrophysics Data System

1995ApJ...441..603B

and the GC sources, compare the GC sources to observed spectra of other types of massive evolved stars from the literature, and attempt to place the GC sources in the H-R diagram.

Libonate et al. (1995) have also recently obtained K band spectra of nine GC sources, including seven of the eight sources we have observed at K, and H band spectra for three GC sources, including the AF source which we have observed at H. Our K band spectra are higher spectral resolution and higher signal-to-noise than the spectra they present for five of the seven sources observed in common.

1.1. *The Ofpe/WN9 Class*

The LMC Ofpe/WN9 stars were first classified by Walborn (1977) and they now number 10 stars in all (Bohannan & Walborn 1989; hereafter BW). These stars are believed to be precursors to the Wolf-Rayet stage and hence are likely to be helium enriched and massive (it is thought that the LBV, Ofpe/WN9, and Wolf-Rayet [WR] classes form an evolutionary sequence; see BW and Humphreys & Davidson 1994, for example). P Cygni profiles in the optical spectra clearly indicate massive outflows from the LMC objects. In addition, the LMC sources have bolometric luminosities and temperatures that place them among the most massive stars ($>30\ M_{\odot}$) in the H-R diagram (MHH). The K band spectra of the present LMC stars are a subset of those first presented by MHH and include three Ofpe/WN9 stars and two early supergiants with He I 2.06 μm/Br$\gamma > 1$. H and K spectra were also presented by McGregor, Hyland, & Hillier (1988, MHH2) for a number of early-type galactic emission-line stars. Several of these stars appear similar to the LMC Ofpe/WN9 stars in the K band. Indeed, one of them, AG Car, may be classified as Ofpe/WN9 by its optical spectrum (Stahl 1986). These NIR spectra are the basis for classification of the GC sources as "He I stars."

Recently, Crowther, Hillier, & Smith (1994) have completed detailed wind (WR like) models for four of the LMC Ofpe/WN9 stars (none from the present sample) and the galactic WN9 star WR108. The detailed spectral types of the LMC stars are changed by Crowther et al. based on new optical spectra, to WN9–10 types. While important for understanding the precise links between evolutionary phases of massive stars, these changes do not affect our comparative analysis of the GC sources. The model results of Crowther et al. are in general agreement with the previous work presented by MHH.

The defining characteristic of the Ofpe/WN9 stars in the K band has been taken as a He I 2.06 μm/Brγ integrated line flux ratio greater than one, sometimes accompanied by He I 2.11 μm emission. Beyond this simple criterion, what more can quantitatively be said regarding the nature of the GC sources in the absence of optical and UV spectra? To answer this question, we have analyzed the H I and He I emission lines in the LMC stars and those in the GC for a direct comparison.

2. OBSERVATIONS AND DATA REDUCTION

The majority of the observations were obtained on the nights of 1993 July 11 and 12 and 1993 September 6 and 22 on the CTIO 4 m telescope. The observations were made using the Ohio State Infrared Imager/Spectrometer (OSIRIS; DePoy et al. 1993) in low-resolution mode ($R \approx 570$). OSIRIS employs a 256 × 256 HgCdTe array and may be used in cross-dispersed mode (simultaneous coverage of J, H, and K bands). The GC sources were observed solely in the K band (except AF) with a 120″ × 1.″3 slit. The AF source and comparison stars were observed in cross-dispersed mode with a 20″ × 1.″3 slit. The spatial scale was 0.″45 pixel^{-1}.

In July, we observed the seven GC He I sources listed in Table 1 with a critically sampled (FWHM ≈ 2 pixel) spectral coverage of approximately 1.9–2.4 μm (19.4 Å pixel^{-1}). The data were taken by first centering on the source IRS 16 SW. The east–west oriented slit was then stepped north–south across the central 15″ in 1.″5–2″ increments. OSIRIS can be easily switched from spectroscopic to imaging mode in real time at the telescope. We recorded several H and K band images during the course of obtaining spectra in order to effectively identify individual sources in the long-slit spectral images. In September, we observed the AF source and the representatives of galactic and LMC emission line stars listed in Table 2. In the present work, we discuss only the H (1.45–1.84 μm) and K (1.9–2.4 μm) spectra for the sources in Table 2, as our goal is to investigate the NIR spectra of the GC sources for which we have no data shortward of H due to interstellar extinction. Each of these sources was individually centered in the cross-dispersed slit.

An additional high-resolution ($R \approx 1350$ at 2.2 μm) spectrum of the GC He I source IRS 13 was obtained in 1994 June with OSIRIS on the CTIO 4 m telescope. The high resolution slit is approximately 0.″5 × 45″. The spatial scale in high resolution was approximately 0.″17 pixel^{-1}.

Basic data reduction tasks were accomplished with standard packages included in IRAF.[3] Each image was sky-subtracted and then flat-fielded using appropriate domeflats.

After flat-fielding, the GC K band (noncross-dispersed) spectra were corrected for anamorphic demagnification by using IRAF "GEOMAP" and "GEOTRAN." This effect, in which the spectrum shifts in the wavelength dimension as a function of spatial position along the slit (resulting in a maximum shift of 5 pixels from slit center to end) was corrected for by deriving a map from the measured positions of OH sky lines along the spatial and spectral dimensions. The transformation from this map to a uniform spectral response along the slit was then applied to each image.

After transformation, each image was ratioed by a secondary flat-field image to remove low-order variations (peak amplitude approximately 30%) due to scattered light in the domeflats. The scattered light remains constant to a few percent from night to night in the domeflats; therefore, all the GC noncross-dispersed K band spectra were ratioed by the same secondary flat. This flat was constructed by building a two-dimensional image from 22 spectra of SAO 191522 taken over a roughly uniform grid along the spatial dimension. Each spectrum was fitted with a low-order polynomial. These low-order fits were combined into a single image and a two-dimensional surface fit to them, resulting in the secondary flat field. Comparison of different measurements of the same star taken at different positions along the slit shows that the low-order variations introduced by the scattered light are reduced from about 30% to about ±5%.

The cross-dispersed slit is much smaller than the normal low-resolution slit so no correction for anamorphic demagnification is required. In addition, all the objects observed in cross-dispersed mode were measured approximately 8–10 times uniformly spaced along the slit. Averaging these measurements effectively removed any low-order variations due to the scattered light in the domeflats.

[3] IRAF is distributed by the National Optical Astronomy Observatories.

© American Astronomical Society • Provided by the NASA Astrophysics Data System

1995ApJ...441..603B

TABLE 1

GALACTIC CENTER LINE MEASUREMENTS

Object	Line (μm)	FWHM[a] (km s^{-1})	W_λ (Å)	Line Flux[b]	Line/Brγ	$\dot{M}$[c]
AF	Br12 1.6412	1200	23	1.5E−12	0.55	...
	Br11 1.6810	850	15	1.1E−12	0.39	...
	He I 1.7007	750	38	2.5E−12	0.92	...
	Br10 1.7367	1000	31	2.0E−12	0.71	...
	He I 2.0587	800	249	8.0E−12	2.88	...
	He I 2.1127	700	29	8.8E−13	0.32	...
	Brγ 2.1661	1000	98	2.8E−12	1.00	1.00
AHH NW	He I 2.0587	1200	109	1.8E−12	2.87	...
	He I 2.1127	1150	37	5.8E−13	0.91	...
	Brγ 2.1661	1200	42	6.3E−13	1.00	0.33
IRS 16 C.....	He I 2.0587	700	17	1.5E−12	2.08	...
	Brγ 2.1661	800	9	7.4E−13	1.00	0.37
IRS 16 NE	He I 2.0587	550	17	4.1E−12	3.43	...
	Brγ 2.1661	600	6	1.2E−12	1.00	0.53
IRS 16 NW.....	He I 2.0587	750	11	7.9E−13	1.89	...
	Brγ 2.1661	900	7	4.2E−13	1.00	0.24
IRS 16 SW	He I 2.0587	700	8	2.0E−12	2.03	...
	Brγ 2.1661	...	4	9.8E−13	1.00	0.46
IRS 1 W	Brγ 2.1661	550	4	4.8E−13	1.00	...
IRS 13	He I 2.0587	950	37	4.2E−12	1.19	...
	He I 2.1127	1800	22	2.5E−12	0.71	...
	Brγ 2.1661	750	31	3.5E−12	1.00	1.19

[a] Observed full width at half-intensity, uncorrected for instrumental broadening. Instrumental width $\approx$565 km s^{-1} at 2.06 μm, 515 km s^{-1} at 1.70 μm. No values appear for lines for which the derived value was significantly less than the instrumental width; see text.

[b] Ergs cm^{-2} s^{-1}. Corrected for adopted reddening shown in Table 4. Estimated uncertainties are $\approx \pm$ 30% for He I 2.06 μm and 30%–80% for the Br lines; see text.

[c] Mass loss relative to AF. See text.

Source spectra were extracted by synthesizing apertures traced along the spectral dimension and then summing the flux in 4–5 pixels along the spatial dimension to form one-dimensional spectra. This aperture size ($\approx$2.″3) may be compared to the typical seeing which was generally between 1″ and 2″. The *K* band cross dispersed spectral features can be broadened by about 10% by this procedure. The *H* band spectra are broadened by less than this amount. In addition, each spectrum had "background apertures" located approximately 1.″5–5″ on one or both sides of the source spectrum. An average background was determined from these 1–2 pixel wide apertures at each wavelength and subtracted from the source spectrum. Determination of this background is critical in assessing the spectral properties of the GC sources which are contaminated by nearby diffuse emission and unresolved stellar light.

Each spectrum was ratioed by the spectrum of a hot star, or atmospheric standard star, to remove telluric absorption features. Brγ (2.16 μm) absorption in the standards was corrected by estimating a linear continuum across the feature. The H I Brackett series absorption lines in the *H* band spectra of the atmospheric standards were removed before ratioing by fitting the profiles and strengths of the three strongest features (Br10, Br11, and Br12) and extrapolating to the higher order lines assuming similar properties and relative strengths estimated from Kurucz (1979). The correction of the higher order lines is imperfect and affects the derived strengths of the H I emission (for Br13 and higher order) in the observed sources at a level $\sim$5% of the continuum.

For the GC *K* band spectra (noncross-dispersed) a wavelength shift of 0–0.5 pixel was made before ratioing to adjust the object spectra to the wavelength zero-point of the standard. The shifts in the object spectra result from slit positioning differences between the atmospheric standards (centered in the slit) and the GC spectra which were positioned randomly in the slit as the slit map of the GC region was obtained by uniformly stepping the slit. The positioning differences lead to wavelength shifts because the incident angle on the diffraction grating is different. The magnitude of the shift was estimated by cross-correlating the object versus the atmospheric standard using only the region of the spectra where strong telluric features dominate ($\lambda > 2.26$ μm). This shift was found to be consistent with the value derived by minimizing the residual features in the strong telluric CO_2 near 2 μm by trial and error shifting and ratioing. These small shifts were then used to interpolate the object spectrum to the zeropoint of the atmospheric standard which was set by the standard's intrinsic Brγ absorption. This procedure was not used for the cross-dispersed data since the sources were centered in the slit.

The object spectra were flux-calibrated by multiplication of a blackbody spectrum appropriate to the atmospheric standards and by setting the 2.2 μm and 1.65 μm flux densities equal to the values derived from broad-band photometry. The photometry and references are given in Table 4. Wavelength calibration was determined from analysis of OH sky lines of known wavelength (Oliva & Origlia 1992). The relative line positions are accurate to $\lesssim$40 km s^{-1}, but the zeropoint for any given nights is certain only to $\sim \pm$ 200 km s^{-1} due to uncertainty in accounting for slit positioning differences discussed above and uncertainty in measuring the zeropoint for any particular atmospheric standard.

The high-resolution spectrum of IRS 13 was reduced similarly to the low-resolution data except that no secondary flat field was used, nor were any shifts made to the spectrum before ratioing by the atmospheric standard star. These additional steps were not required since a series of measurements were

© American Astronomical Society • Provided by the NASA Astrophysics Data System

1995ApJ...441..603B

TABLE 2

GALACTIC AND LMC STAR LINE MEASUREMENTS

Object	Line (μm)	FWHM[a] (km s^{-1})	W_λ (Å)	Line Flux[b]	Line/Brγ	$\dot{M}$[c]
WR 122	Br12 1.6412	950	11	1.6E−12	0.36	
	Br11 1.6810	750	11	1.7E−12	0.38	
	He I 1.7007	500	113	1.7E−11	3.82	
	Br10 1.7367	750	12	1.9E−12	0.43	
	He I 2.0587	600	715	1.5E−10	33.94	
	He I 2.1127	500	26	5.8E−12	1.29	
	Brγ 2.1661	900	20	4.5E−12	1.00	
WR 85a	Br12 1.6412	800	8	8.6E−13	0.52	
	Br11 1.6810	800	8	9.2E−13	0.56	
	He I 1.7007	600	34	3.8E−12	2.27	
	Br10 1.7367	700	8	9.4E−13	0.57	
	He I 2.0587	650	300	3.6E−11	21.79	
	He I 2.1127	550	11	1.3E−12	0.79	
	Brγ 2.1661	1000	14	1.7E−12	1.00	
HD 269445.....	Br12 1.6412	950	10	1.5E−13	1.24	
	Br11 1.6810	1100	9	1.3E−13	1.02	
	He I 1.7007	550	7	8.9E−14	0.73	
	Br10 1.7367	950	10	1.3E−13	1.04	
	He I 2.0587	600	37	3.2E−13	2.63	
	He I 2.1127	...	5	4.3E−14	0.35	
	Brγ 2.1661	1100	16	1.2E−13	1.00	1.36
HD 269582.....	Br12 1.6412	600	9	3.7E−14	0.32	
	Br11 1.6810	700	14	5.3E−14	0.46	
	He I 1.7007	500	23	8.2E−14	0.71	
	Br10 1.7367	750	20	7.0E−14	0.61	
	He I 2.0587	550	19	3.5E−14	0.30	
	He I 2.1127	600	21	3.5E−14	0.31	
	Brγ 2.1661	850	71	1.2E−13	1.00	1.31
HD 269687.....	Br12 1.6412	700	5	1.3E−14	1.11	
	Br11 1.6810	...	2	4.2E−15	0.36	
	He I 1.7007	...	4	9.3E−15	0.79	
	Br10 1.7367	500	3	6.9E−15	0.59	
	He I 2.0587	450	30	3.5E−14	3.02	
	He I 2.1127	900	4	4.6E−15	0.39	
	Brγ 2.1661	550	11	1.2E−14	1.00	0.23
HD 37836	Br12 1.6412	700	9	1.4E−13	0.90	
	Br11 1.6810	500	7	9.8E−14	0.64	
	He I 1.7007	...	6	7.6E−14	0.49	
	Br10 1.7367	...	7	9.2E−14	0.60	
	He I 2.0587	450	39	3.4E−13	2.21	
	He I 2.1127	900	3	2.7E−14	0.18	
	Brγ 2.1661	450	20	1.5E−13	1.00	1.61
HD 268840.....	Br12 1.6412	750	14	2.7E−14	1.34	
	Br11 1.6810	550	9	1.9E−14	0.91	
	He I 1.7007	500	10	1.9E−14	0.93	
	Br10 1.7367	600	12	2.1E−14	1.04	
	He I 2.0587	550	47	5.1E−14	2.49	
	He I 2.1127	...	3	4.3E−15	0.21	
	Brγ 2.1661	650	19	2.0E−14	1.00	0.36
WR 108	Br12 1.6412	1100	5	1.1E−12	0.46	
	Br11 1.6810	1000	3	6.7E−13	0.28	
	He I 1.7007	950	7	1.5E−12	0.62	
	Br10 1.7367	1100	9	1.6E−12	0.68	
	He I 2.1127	850	15	1.5E−12	0.61	
	Brγ 2.1661	1100	26	2.4E−12	1.00	0.45
S Dor	Br12 1.6412	800	12	6.2E−13	0.77	
	Br11 1.6810	850	16	7.6E−13	0.94	
	Br10 1.7367	550	14	6.0E−13	0.75	
	Brγ 2.1661	450	50	8.1E−13	1.00	5.59

[a] Observed full width at half intensity, uncorrected for instrumental broadening. Instrumental width $\approx$565 km s^{-1} at 2.06 μm, 515 km s^{-1} at 1.70 μm. No values appear for lines for which the derived value was significantly less than the instrumental width; see text.

[b] Ergs cm^{-2} s^{-1}. Corrected for adopted reddening shown in Table 4. Estimated uncertainties are $\approx \pm$ 30% for He I 2.06 μm and 30% to 80% for the Br lines; see text.

[c] Mass loss relative to AF. See text.

© American Astronomical Society • Provided by the NASA Astrophysics Data System

1995ApJ...441..603B

made uniformly along the slit, and IRS 13 was centered in the slit. The high-resolution spectrum was wavelength calibrated like the low-resolution data with the zeropoint set so that Brγ had the same observed wavelength as the low-resolution spectrum.

The final spectra are shown in Figures 1–4. The low-amplitude periodic modulation of the continuum evident in some of the spectra is due to fringing inherent to OSIRIS (see IRS 16 SW, for example). The fringe pattern is inclined relative to the wavelength dimension (i.e., the fringes change phase as a function of position along the image spatial dimension). The fringe period is approximately 2–4 pixel^{-1} in the wavelength dimension and decreases from blue to red wavelengths. The fringes in Figures 1–3 result from a combination of fringing observed in both the object and atmospheric standards. The fringing amplitude can be as high as 3% of the continuum, but is typically less for two reasons. First, fringes in the atmospheric standards tend to average out when multiple measurements are co-added and second, fringes in the atmospheric standard may cancel out fringes in the object.

The emission lines in each spectrum were analyzed with the LINER program (written by Richard Pogge of OSU), an interactive spectral line analysis program in use at Ohio State. For each line, a best-fit Gaussian is determined from a least-squares fit. The analysis includes a low-order polynomial fit to the continuum which is made independently of individual line fits by selecting continuum points clear of features over a 0.1–0.2 μm range. Derived quantities from the best fit for each line are shown in Tables 1–3.

The line FWHMs are the best-fit values to the observed profiles, uncorrected for instrumental broadening. We estimate the uncertainty in a derived FWHM to be approximately ± 50 km s^{-1} from the scatter about the expected instrumental width for a number of unresolved, or marginally resolved He I 2.06 μm and Brγ lines. Some lines have no quoted FWHM. These are typically those with small equivalent width where the signal to noise was inadequate to yield a FWHM. Several stronger lines also had FWHM which were about 2 σ smaller than the instrumental width, which is possibly due to the atmospheric correction for these stars.

The line fluxes are corrected for interstellar extinction. We adopt $A_K = 3.0$ mag for the GC He I sources so a direct comparison can be made with the results of Krabbe et al. (1991). For the other sources, the adopted extinction follows from the $E(B-V)$ given in the reference cited in Table 4 and a power-law fit to the interstellar extinction curve of Rieke & Lebofsky (1985). The uncertainties for the line fluxes are dominated by systematic effects which include fringing inherent to OSIRIS, using published photometry for the flux calibration (several of the sources are known variables, and most are expected to vary), incomplete cancellation of telluric features near the 2.06 μm He I line, and errors in correction of the intrinsic spectral

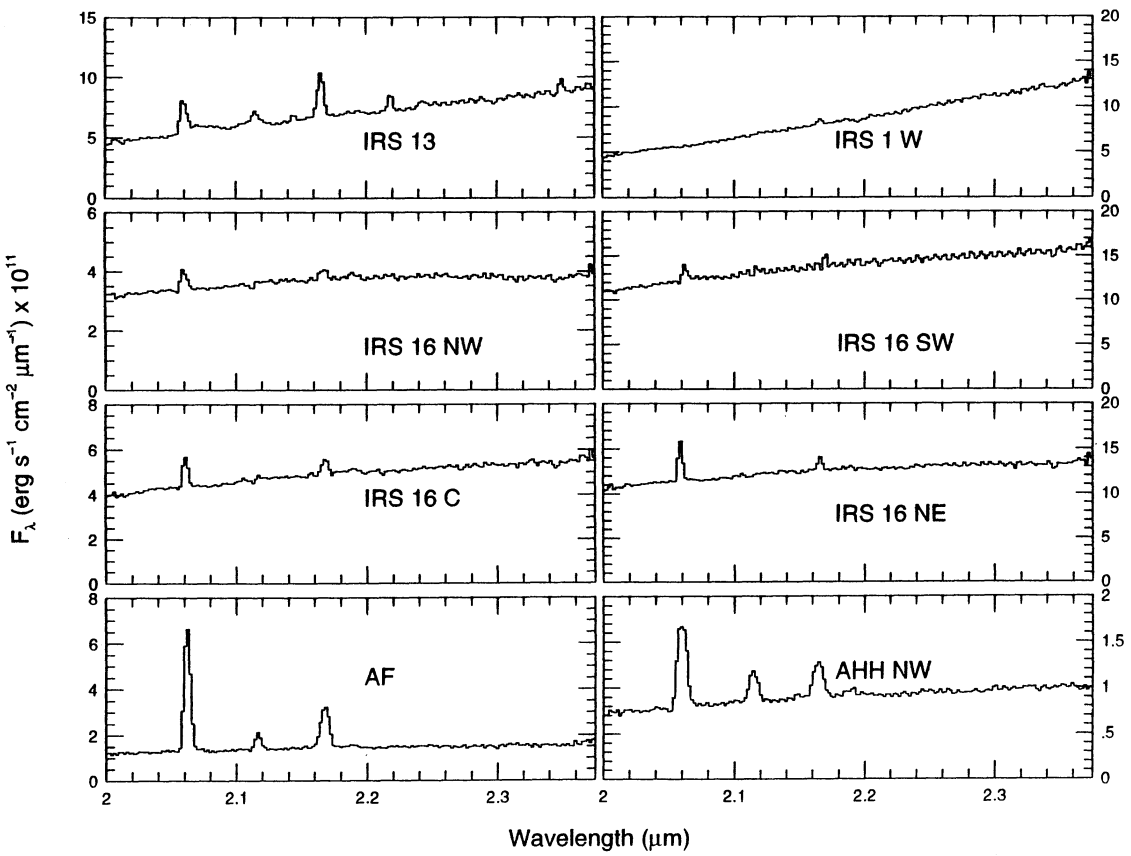

FIG. 1.—K band spectra of He I emission-line sources in the Galactic center showing the He I 2.06 μm and Brγ (2.17 μm) emission lines. The resolution ($\lambda/\Delta\lambda$) is approximately 570 at 2.2 μm. Several sources also show He I emission at 2.11 μm. The lines near 2.15 μm, 2.22 μm, 2.24 μm, and 2.35 μm in IRS 13 are due to [Fe III]. These spectra were extracted from $\approx 1''.8 \times 1''.4$ apertures and include background subtraction from nearby ($\lesssim 2''$) apertures. The low-amplitude periodic modulation of the continuum evident in some of the spectra is due to fringing inherent to OSIRIS (see IRS 16 SW, for example). Note that the emission lines in several of the sources are resolved (He I 2.06 μm FWHM > 565 km s^{-1}).

© American Astronomical Society • Provided by the NASA Astrophysics Data System

1995ApJ...441..603B

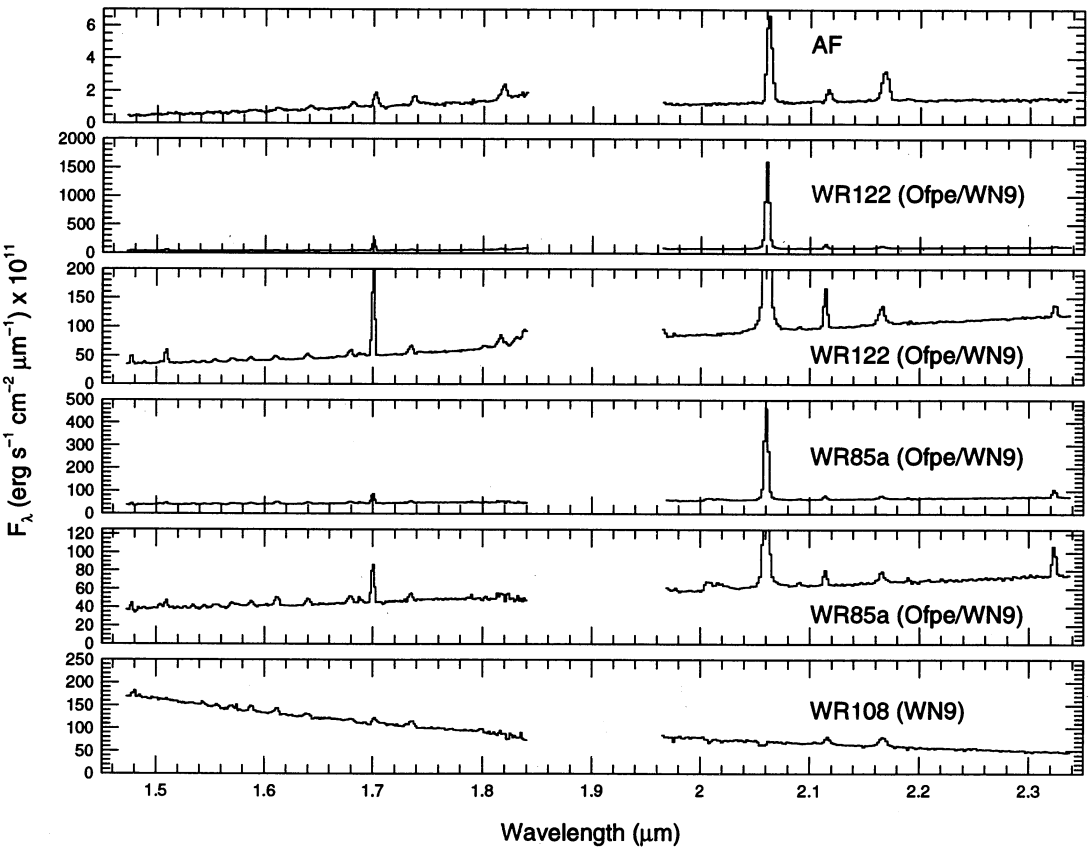

FIG. 2.—*H* and *K* band spectra of He I emission-line sources in the Galaxy showing the He I 1.70 μm and 2.06 μm lines and Brackett series emission lines. Reliable detections are made for Brγ (2.17 μm), Br9 (1.82 μm), Br10 (1.74 μm), Br11 (1.68 μm), and Br12 (1.64 μm). The weaker Br lines may be due to imperfect correction of intrinsic H I absorption in the standards used to correct for atmospheric absorption. The spectra for WR 85a and WR 122 are shown twice with two different scales for clarity. The lines near 1.69 μm and 2.09 μm in WR 85a and WR 122 are due to Fe II. The line present at 232 μm in WR 85a and WR 122 is unidentified. These spectra were extracted from ≈2″.3 × 1″.4 apertures and include background subtraction from nearby (≲5″) apertures. The resolution ($\lambda/\Delta\lambda$) is approximately 570 at 1.65 and 2.2 μm.

features of the atmospheric standards. Comparison of our 2.06 μm He I line fluxes to the published values for the LMC stars (excluding HD 269582, see § 3.3 below) shows typical agreement to ±30%. The H I lines measured at *H* are more uncertain. A typical uncertainty in the Br10, 11, and 12 lines ranges from 10% to 80%, due mainly to errors in the correction to the same features in the atmospheric standards. Br13 can be off by a factor of 2 and is not reliably detected in the majority of sources. The uncertainty arising due to correction of Brγ in the atmospheric standard is less because Brγ is well defined and unblended by other intrinsic features in the standard star continuum. Comparison to the Brγ line fluxes given in MHH for the same stars we have observed shows agreement to better than a factor of 2.

TABLE 3

IRS 13 HIGH-RESOLUTION LINE MEASUREMENTS

Line (μm)	FWHM[a] (km s^{-1})	W_λ (Å)	Line Flux[b]	Line/Brγ
He I 2.0587	1030	38	4.7E−12	1.07
? 2.1045	990	4	4.7E−13	0.11
He I 2.1127	850	14	1.6E−12	0.37
[Fe III] 2.1457	380	2	2.6E−13	0.06
Brγ 2.1661	570	37	4.4E−12	1.00
He I? 2.1851	520	1	1.4E−13	0.03
He II? 2.1891	420	1	1.2E−13	0.03
[Fe III] 2.2178	420	6	6.1E−13	0.14

[a] Observed full width at half-intensity uncorrected for instrumental broadening. Instrumental width ≈240 km s^{-1} at 2.06 μm.

[b] Ergs cm^{-2} s^{-1}. Corrected for adopted reddening shown in Table 4. These measurements are consistent with the low-resolution measurements in Table 1; see text.

The line measurements of the high-resolution spectrum of IRS 13 show excellent agreement with those from the low-resolution data. The flux measurements made with quite different spatial scales and slit widths are within 10% and 25% for He I 2.06 μm and Brγ, resspectively.

We have compared our dereddened line fluxes for the AF source, AHH-NW, IRS 13, IRS 1 W, IRS 16 NE, IRS 16 C, and IRS 16SW with the results of Krabbe et al. (1991), and our equivalent widths and line fluxes for AF, IRS 13, IRS 1 W, IRS 16 NE, IRS 16 NW, IRS 16 C, and IRS 16 SW with the results of Libonate et al. (1995). The comparison shows modest agreement. Our fluxes agree to 50% or better with those of Krabbe et al. for AF, AHH-NW, IRS 13, IRS 16 NE, and IRS 16 SW; the two remaining sources, IRS 1 W and IRS 16 C, do not agree well. Our fluxes agree with those of Libonate et al. to better than a factor of 2 for only IRS 16 C and IRS 16 SW, while our equivalent widths agree to better than a factor of 2 with those of Libonate et al. for only IRS 13, IRS 16 NE, and IRS 16 C. Different choices of background apertures and beam sizes will affect both the line fluxes and equivalent widths.

© American Astronomical Society • Provided by the NASA Astrophysics Data System

1995ApJ...441..603B

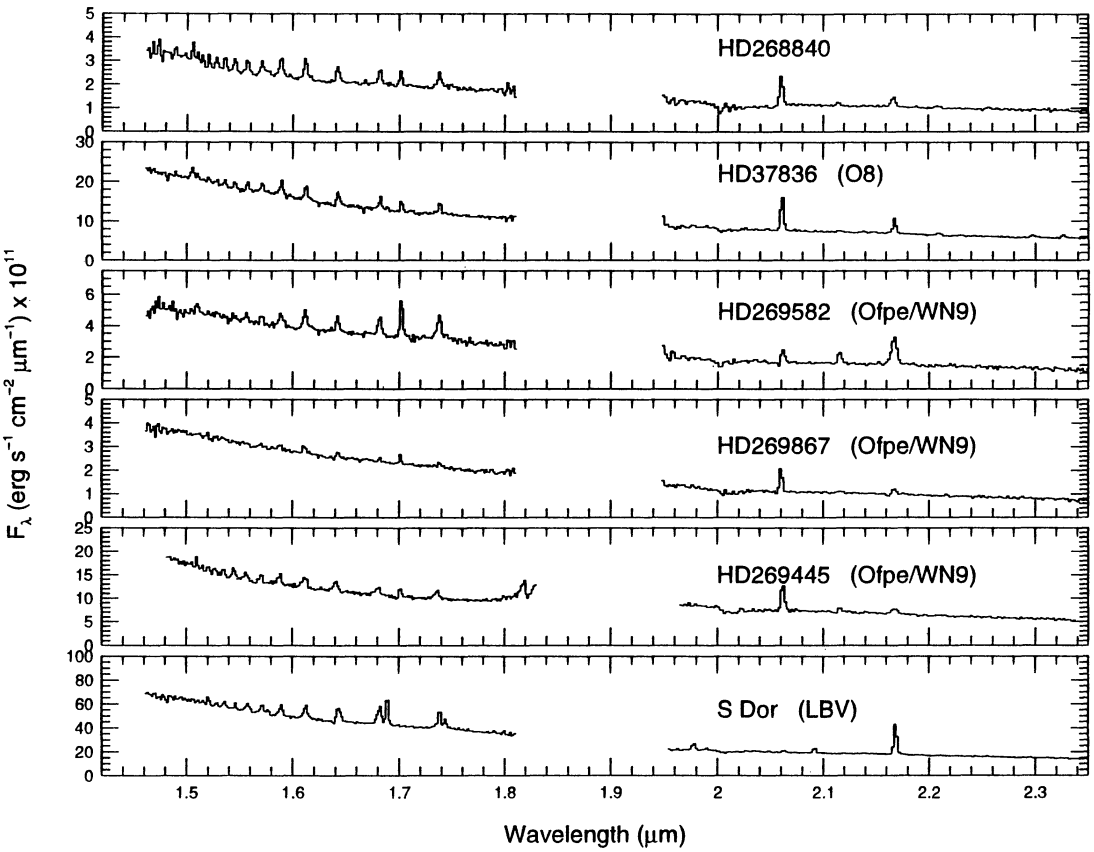

FIG. 3.—Same as Fig. 2 but for He I emission-line sources in the LMC. Spectra of the luminous blue variable, S Dor, which shows no He I, is shown for comparison. The lines near 1.69 μm, 1.74 μm, and 2.09 μm are due to Fe II. The Na I (2.21 μm) and CO (2.3 μm) emission reported by MHH for HD 37836 are seen in our spectrum. The Na I line may also be present in the spectrum of HD 268840.

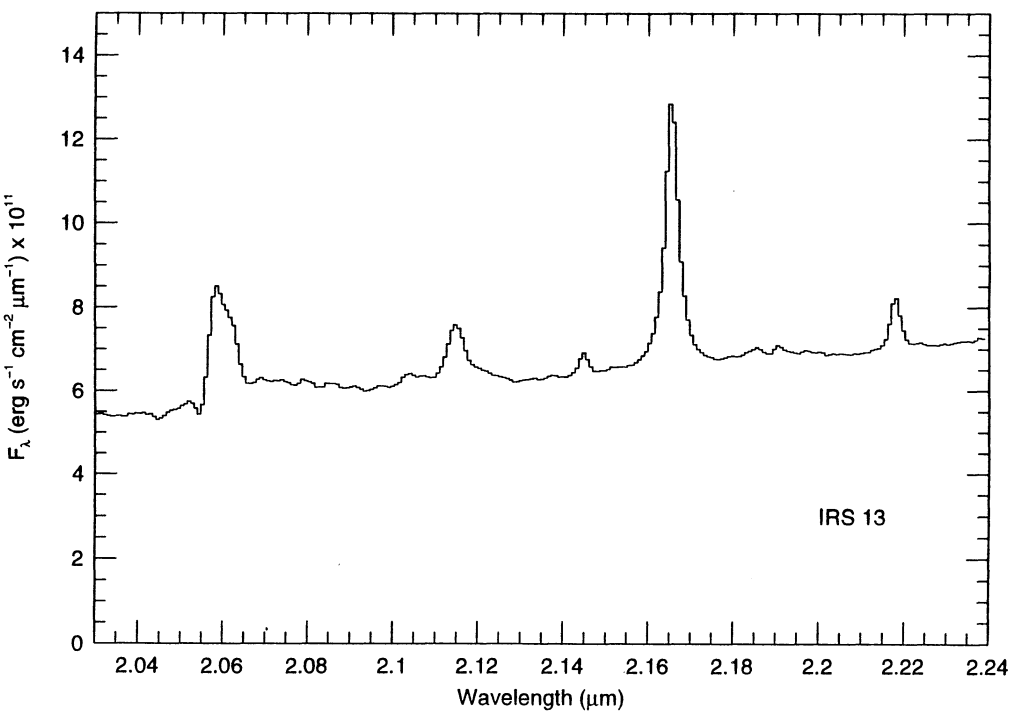

FIG. 4.—High-resolution ($R \approx 1350$, 120 km s^{-1} pixel^{-1}) spectrum of IRS 13. Note the emission to the red of the He I 2.06 μm and 2.11 μm lines. The lines at 2.15 and 2.22 μm are due to [Fe III]. This spectrum was extracted from a $\approx 0\farcs5 \times 1\farcs0$ aperture and includes background subtraction from nearby ($\lesssim 2''$) apertures on either side of it. All of the emission lines are resolved (observed FWHM $\gtrsim$ 240 km s^{-1}).

© American Astronomical Society • Provided by the NASA Astrophysics Data System

1995ApJ...441..603B

TABLE 4

STELLAR PHOTOMETRY AND PARAMETERS

Object	Type	K	H	$H-K$	A_K[a]	$(H-K)_0$	D (kpc)	M_K	M_{bol}	BC_K	T_{eff}	Reference[b]
HD 269445	Ofpe/WN9	9.56	9.98	0.42	0.20	0.30	46.8	−8.99	−11.60	−2.61	4.46	1, 2, 2, 2, 3, 2, 2
HD 269687	Ofpe/WN9	11.58	11.65	0.07	0.06	0.03	46.8	−6.83	−9.80	−2.97	4.47	1, 2, 2, 2, 3, 2, 2
HD 269582	Ofpe/WN9	11.08	11.24	0.16	0.06	0.12	46.8	−7.33	−9.25	−1.92	4.40	1, 2, 2, 2, 3, 2, 2
SK 67-266	Ofpe/WN9	11.88	12.02	0.14	0.05	0.11	46.8	−6.52	−9.62	−3.10	4.48	1, 2, 2, 2, 3, 2, 2
Hen S9	Ofpe/WN9	11.47	11.85	0.38	0.09	0.33	46.8	−6.97	−8.87	−1.90	4.46	1, 2, 2, 2, 3, 4, 4
HD 37836	O8	9.40	9.73	0.33	0.03	0.31	46.8	−8.98	−10.50	−1.52	4.45	5, 6, 6, 2, 3, 2, 2
HD 268840	...	11.49	11.88	0.39	...	...	46.8	−6.86	...	...	...	2, 2, 3
S Dor	LBV	8.61	8.4	−0.21	0.02	−0.22	46.8	−9.76	−9.80	−0.04	4.25	7, 8, 8, 8, 3, 8, 8
P Cyg	LBV	3.34	3.51	0.17	0.21	0.05	1.8	−8.15	−9.90	−1.75	4.28	7, 9, 9, 10, 10, 10
HR Car	LBV	5.34	5.51	0.17	0.4	−0.06	5.0	−8.55	−8.90	−0.35	4.15	7, 11, 11, 11, 12, 12, 12
He 3–519[c]	...	7.42	7.63	0.21	0.46	−0.06	8.0	−7.56	−10.80	−3.24	4.50	7, 13, 13, 7, 14, 7, 7
Eta Car	LBV	1.14	2.58	1.44	0.4	1.21	2.5	−11.25	−11.5	−0.25	4.4	7, 9, 9, 11, 11, 7, 7
AG Car	LBV	5.76	6.11	0.35	0.2	0.23	6.0	−8.33	−10.80	−2.47	4.48	7, 11, 11, 15, 15, 15, 15
WR 108	WN9	7.13	7.4	0.27	0.45	0.01	5.0	−6.81	−9.9	−3.09	4.48	16, 17, 17, 17, 4, 4, 4
WR 122	Ofpe/WN9	6.45	8.49	2.04	0.81	1.57	...	...	...	...	...	16, 17, 17, 17
WR 85a	Ofpe/WN9	6.96	8.55	1.59	0.64	1.22	...	...	...	...	...	16, 17, 17, 17
AF	...	10.95	12.71	1.76	3.00	0.01	8.0	−6.57	...	...	...	18, 18, 19, 20
AHH NW	...	11.60	13.61	2.01	3.00	0.25	8.0	−5.92	...	...	...	18, 21, 19, 20
IRS 16 C.....	...	9.78	11.82	2.04	3.00	0.29	8.0	−7.74	...	...	...	22, 22, 19, 20
IRS 16 NE	...	8.76	10.83	2.07	3.00	0.32	8.0	−8.76	...	...	...	22, 22, 19, 20
IRS 16 NW.....	...	10.07	11.93	1.86	3.00	0.10	8.0	−7.45	...	...	...	22, 22, 19, 20
IRS 16 SW	...	8.67	11.5	2.83	3.00	1.08	8.0	−8.85	...	...	...	22, 22, 19, 20
IRS 1 W	...	9.20	11.17	1.97	3.00	0.22	8.0	−8.32	...	...	...	23, 24, 19, 20
IRS 13	...	9.40	11.17	1.77	3.00	0.01	8.0	−8.12	...	...	...	23, 24, 19, 20

[a] A_K determined from $E(B-V)$ or A_V assuming $R = 3.1$ and the interstellar reddening curve of Rieke & Lebofsky 1985.

[b] References are listed in order of type, K, H, A_K, D, M_{bol}, and T_{eff}: (1) BW, (2) MHH; (3) Reid & Strugnell 1986; (4) Crowther et al. 1994; (5) Hutchings, 1980; (6) Stahl et al. 1985; (7) Humphreys & Davidson 1994; (8) Leitherer et al. 1985; (9) Allen 1973; (10) Lamers et al. 1983; (11) MHH2; (12) van Genderen et al. 1991; (13) Allen & Glass 1974; (14) Davidson et al. 1993; (15) Humphreys et al. 1989; (16) van der Hucht et al. 1988; (17) Williams et al. 1987; (18) DePoy, private communication, (19) Wade et al. 1990; (20) Reid 1989; (21) Present work, (22) DePoy & Sharp 1991, (23) Simon et al. 1990; (24) Rieke et al. 1989.

[c] Possible LBV (Humphreys & Davidson 1994).

Which of these will be more affected will depend on the source being compared and the particular choices made.

Line and continuum variations are expected for mass-losing stars, but differences in the placement and size of source and sky apertures are more likely the cause of differences in the observed line fluxes and equivalent widths in the GC where source crowding is a serious problem.

3. DISCUSSION

The fundamental problem is assessing the nature of the He I sources at the GC is that we can observe only the red end (NIR wavelengths or longer) of their spectra. If these objects are massive evolved stars which live in the upper part of the H-R diagram, we may expect significant differences among their observed spectra based on experience with WR, LBV, and Ofpe/WN9 stars which have much more extensive spectral coverage (see the review of LBVs by Humphreys & Davidson 1994, for example). The task then, is to discern the nature of the GC He I sources using only a fraction of the wavelength coverage available when studying their visible (proposed) counterparts.

The following sections explore the similarities and differences between the comparison stars and GC He I sources. We first discuss the H I lines to establish more firmly the wind nature of the GC sources. We then move to the He I lines which provide the most dominant features in the GC spectra. We end with discussions of the mass-loss rates for the GC sources and their location in the H-R diagram.

3.1. H I *Lines: AF vs. Galactic and LMC Stars*

The Brackett line equivalent widths (W_λ) are consistently larger in AF (this paper, Table 1; Libonate et al. 1995) than any of the comparison stars (this paper, Table 2). The Brackett line to Brγ ratios for the comparison stars show a large range of values which encompass the ratios of AF. We find no relationship between the observed line ratios and the known physical parameters of the comparison stars. The line ratios in the LMC stars and galactic source WR85a are larger than predicted for case B recombination (Hummer and Storey 1987; $T_e = 10^4$ K, $n_e > 10^4$ cm^{-3}). This suggests that the lines are optically thick (MHH2; Simon et al. 1983). WR 122 is consistent with either high-density ($n_e > 10^9$ cm^{-3}) case B or optically thick line ratios depending on the reddening.

The AF source is consistent with optically thick Brackett line emission if the adopted reddening is large ($A_K \approx 3$) as is typically taken for the GC. It is important to point out that we should expect some NIR excess to be associated with the AF source if it is an Ofpe/WN9 star. The LMC stars are generally consistent with an excess due to free-free emission (MHH), while the two galactic Ofpe/WN9 stars are associated with circumstellar dust (Williams, van der Hucht, & Thé 1987) as can be seen from their rising continua (Fig. 2) and spectral energy distributions given by Williams et al. (their Fig. 4; note that WR 85a = LSS 4005). This means any interpretation of the AF emission lines or NIR colors will be subject to considerable uncertainty. However, it is possible to rule out case B line ratios for AF based upon the measurements of Brγ and Paα reported by Najarro et al. (1994), which indicate that the ratio of Brγ to Paα could only be case B if the extinction at K is significantly *larger* than 3.0 mag. Such a large value is ruled out by the NIR colors of AF (our own unpublished colors: $J = 15.74 \pm 0.06$, $H = 12.71 \pm 0.07$, $K = 10.95 \pm 0.11$, and $L = 9.14 \pm 0.06$) which would then be bluer than a blackbody of any temperature.

© American Astronomical Society • Provided by the NASA Astrophysics Data System

1995ApJ...441..603B

3.2. *The Galactic Center* He I *Emission-Line Sources*

The AF, AHH NW, WR 85a, and WR 122 stars have about an order of magnitude greater He I 2.06 μm equivalent width than the LMC stars. The W_λ ranges from 109 Å to 715 Å for these stars (this paper, Table 1; Libonate et al. 1995) which may be compared to the average $W_\lambda = 34 \pm 10$ Å for the LMC stars (this paper, Table 2). The four galactic/GC sources also show larger W_λ in the 1.700 μm line with the galactic/GC objects exhibiting $W_\lambda \gtrsim 20$ Å (this paper, Tables 1 and 2; Libonate et al. 1995) while the LMC stars show $W_\lambda \lesssim 10$ Å (this paper, Table 2). The He abundance predicted by Najarro et al. (1994) for AF is larger than the values derived by Crowther et al. (1994) for the LMC stars: He/H by number of 1.3 ± 0.3 compared to 0.3 ± 0.1. Theoretical models for massive stars (Maeder 1990) predict that He/H at the surface will change by large amounts over short evolutionary periods, so this difference may not be significant. The observed difference in W_λ's between the spectrum of AF (and the other galactic sources) and the LMC comparison stars, may also point to differences in the mass loss rate, ionization structure and effective temperature, as well as the He/H abundance ratio. All of these strongly affect the He I 2.06 μm line flux (Najarro et al. 1994; see also Shields 1993). Accurate W_λ's provide strong model constraints since they are not directly affected by reddening.

The remainder of the GC sources have much smaller equivalent widths, on average a factor of 2 less than the LMC stars (this paper; Libonate et al. 1995). Eckart et al. (1993) have proposed that the IRS 16 cluster is composed of about 25 stars. However, the lunar occultation results of Simon et al. (1990) and Simons, Hodapp, & Becklin (1990) indicate IRS 6 C, NE, SW, and NW emit the majority of the flux observed and are compact objects less than 200 AU in size. If the He I emission is in fact associated with fainter objects near the bright IRS 16 components, then the lower W_λ compared to AF, AHH NW, and the other comparison stars could result from source crowding. However, if the He I sources (coincident with IRS 16) are to have similar equivalent width as AF ($\sim 10 \times$ lower continuum), then they would tend to be underluminous at K, compared to the LMC stars (Table 4), since this would require reducing the continuum flux substantially for the same observed line flux. The observed continuum would then be due to the He I source and other, bright, nonemission-line sources combined.

The level of He I emission in the two galactic WN9/Ofpe stars, WR 85a and WR 122, is remarkable, The He I lines are at least an order of magnitude stronger relative to Brγ than in the other emission-line stars we observed and other emission-line objects in general (e.g., DePoy & Shields 1994). This suggests that regardless of the physical conditions in these two sources, the He to H abundance ratio must be significantly different from the solar value (~ 0.1). For example, the ratio of Brγ to the sum of the singlet and triplet transitions producing He I 2.113 μm emission is expected to be ~ 0.03 for a helium to hydrogen abundance ratio of 0.1, based on recombination rates appropriate for 10^4 K and 10^6 cm^{-3} from Brockelhurst (1972) and Hummer & Storey (1987) and He I branching ratios of Wiese, Smith, & Glennon (1966). Although the applicability of this calculation is difficult to determine given the likelihood the sources have optically thick line emission (see § 3.2), the observed values of the He I 2.113 μm to Brγ emission in WR 122 (~ 1.3) and in WR 85a (~ 0.8) suggests that the He/H abundance ratio in these objects is greater than 1. (Note that we have elected not to base our abundance estimates on the strength of the He I 2.06 μm line emission, which is strongly affected by resonant scattering of the He I $2\,^1P \rightarrow 1\,^1S$ 584 Å line and hence sensitive to geometry, density, dust content, and velocity structure, as well as abundance; see Shields 1993).

Comparison of Tables 1 and 2 shows another difference between the GC and individual sources: all the highest velocity widths are observed in the GC; the galactic and LMC emisson-line stars are unresolved at our resolution. The observed He I velocity widths uncorrected for the instrumental profile range from unresolved to approximately 1200 km s^{-1} (excluding the 2.11 μm line for IRS 13; see below) for the GC sources, while the galactic and LMC comparison stars are unresolved (FWHM $\lesssim 565$ km s^{-1} at 2.06 μm, FWHM $\lesssim 513$ km s^{-1} at 1.70 μm). The measured widths of several comparison stars (WR 122, WWR 85a, and HD 269445) appear marginally resolved, but this is likely due to the extraction technique described above which may broaden the lines by $\sim 10\%$. Our conclusions on the line widths are most firm for the He I widths since the H I lines may suffer from systematic uncertainty due to the reduction procedure as described above and also may be broadened by He I emission and so are not representative of the wind velocity (Najarro et al. 1994). For widths greater than our instrumental resolution, our results for the He I 2.06 μm line width are in good agreement with Krabbe et al. (1991) and Libonate et al. (1995).

Crowther et al. (1994) measure the wind terminal velocity for four of the 10 LMC Ofpe/WN9 stars from He I P Cygni profiles in the UV and IR. All four stars show terminal wind velocities less than 500 km s^{-1}, consistent with our measurements of similar LMC stars. Higher velocities are expected for the hotter WR stars. We find that the highest velocity GC source is AHH NW which has a He I 2.06 μm FWHM of 1200 km s^{-1}, similar to the terminal velocity reported for WR 108 by Crowther et al. (1994). AHH NW is also the faintest He I source we observed. If it were hotter, its bolometric correction could be larger (see below) than the other GC sources. The K band spectra of AHH NW and WR 108 are significantly different; WR 108 shows no He I 2.06 μm emission. However, the models of Crowther et al. for one Ofpe/WN9 star indicate that changes in the ionization structure of the wind (which result from relatively small changes in the stellar input parameters) lead to significant changes in the 2.06 μm emission, causing it to range from essentially no emission to the amount indicated by the observed spectrum. However, the models which reproduce the observed 2.06 μm emission do not reproduce all the important features of the optical spectrum (Crowther et al. do not regard this as a serious problem; see their discussion of the models for the object Sk $-66°40$). Whether similar results would hold for WR 108 is unclear. If large changes in the NIR spectra of these stars can result from small changes in the stellar parameters, the task of identifying the GC sources becomes even more difficult.

The significance of the observed differences in the NIR spectra of AF and AHH NW and the comparison stars is unknown. We might expect that differences in abundance and environment could lead to different physical conditions in the envelopes of these stars. Abundances may play a key role since mass loss is expected to be metallicity dependent (Abbott 1982) and there are differences in abundances between the LMC, and Galaxy, and GC. The LMC is known to be metal-poor relative to the galaxy (e.g., Dufour 1986 and references therein) and there is evidence that the GC be metal-rich (Lacy et al. 1980;

© American Astronomical Society • Provided by the NASA Astrophysics Data System

1995ApJ...441..603B

Shields & Ferland 1994). Likewise, star formation and evolution may proceed differently in the GC where collisional/merger processes are thought to be important between stars and/or stellar remnants (Phinney 1989; Morris 1993).

We close our discussion of the GC K band spectra by pointing out several differences or extensions which our observations reveal relative to previous work. First, the spectral coverage is significantly greater than previous work. The He I 2.113 μm line and full K band continuum are included for eight GC sources. Full K band spectra are also presented by Libonate et al. (1995) for nine GC sources, but at lower spectral resolution than ours. We find no evidence for 2.113 μm emission in the IRS 16 sources with the possible exception of IRS 16 SW, as is shown in Figure 1. Indeed, we may see small absorption at 2.113 μm in IRS 16 NW and IRS 16 C. This is not expected for the Ofpe/WN9 stars, but if present, could be due to contamination by late O or early B stars (Hanson & Conti 1994). Libonate et al. (1995) do not see 2.113 μm emission or absorption in any of the IRS 16 sources.

The spatial scale on OSIRIS allows us to make background subtraction from nearby ($\lesssim 2''$) apertures for all the GC sources. This provides a more accurate estimate of the relative line to continuum flux for the compact point sources and eliminates contributions to the line emission from the diffuse ionized gas. Note the spectrum of IRS 1 W shown in Figure 1. We find no He I emission after background subtraction. The embedded source(s) suggested by Rieke & Lebofsky (1982) and Rieke, Rieke, and Paul (1989) in IRS 1 W does not appear to be a He I emission-line source, contrary to the results of Krabbe et al. (1991) who did not subtract a local background. Libonate et al. (1995), who do subtract a local background, also conclude that IRS 1 W is not a He I emission-line star.

Our observations reveal several important details which the Fabry-Perot data of Krabbe et al. (1991) do not. First, a number of sources show emission to the red of the He I 2.06 μm line, see IRS 13 in Figure 1 for the most prominent example, but IRS 16 NW and SW may also exhibit this behavior. The spectral coverage of Krabbe et al. was insufficient to detect this emission which extends ~ 5000 km s^{-1} to the red in the case of IRS 13. This emission is not included in the line fluxes in Table 1 since it is not clear whether it is a blend of other lines or part of the He I emission. It amounts to 40% of the He I line in IRS 13.

Hillier (1984, 1991) attributed extended emission to the red of optical He II lines in the WN5 star HD 50896 to electron scattering. Asymmetric (red wing) profiles are expected when the wind velocity becomes strong relative to the electron thermal velocity, as is the case of HD 50896. For stars which have wind velocities much smaller than the electron thermal velocity, the profiles are symmetric. This is the case for P Cygni (Bernat & Lambert 1978). The fact that redward emission is not seen in Brγ and that the He I 2.11 μm line appears extended on both the red and blue sides suggests that, at least for IRS 13, the emission might be due to unknown lines. To further investigate this unusual source, we obtained the high-resolution (≈ 120 km s^{-1} pixel^{-1} at 2.06 μm) spectrum shown in Figure 4. The line measurements are shown in Table 3.

The broad wing to the 2.06 μm line is not resolved into individual lines in the high-resolution spectrum of IRS 13. The emission profile appears quite similar in the high and low-resolution spectra. The broad emission near 2.11 μm does split up into two lines separated by about 0.01 μm. The blue component is unidentified. The He I 2.11 μm line profile also appears to exhibit a red wing in the high-resolution spectrum. This strengthens the possibility that a line formation mechanism intrinsic to the IRS 13 outflow is important for the He I lines. We cannot say whether electron scattering is responsible for the formation of the He I red wings, and we note that the Brγ emission clearly does not exhibit profiles like the He I lines. Perhaps Brγ is still contaminated by emission not associated with IRS 13 which masks a red wing. [Fe III] emission (see below) may not be physically associated with the outflow from IRS 13, but does peak quite strongly along this line of sight (Lutz, Krabbe, & Genzel 1993).

Two weak features appear at 2.185 and 2.191 μm in the high-resolution spectrum of IRS 13. The longer wavelength line is possibly due to the He II (10–7). This suggests that the effective temperature for IRS 13 may be similar to the Ofpe/WN9 stars. The Ofpe/WN9 star models of Crowther et al. (1994) for Sk $-66°40$ predict $T_{\rm eff} \approx 29{,}000$ K with small W_λ (1–6 Å) in the He II 2.189 μm line. The line near 2.185 μm may be due to He I $4p\,^1P^0 \rightarrow 7d\,^1D$.

Extended emission from [Fe III] peaks near IRS 13 but may not be otherwise associated with it (Lutz et al. 1993). The lines identified by Lutz et al., $^3G_3 \rightarrow {}^3H_4$ 2.1457 μm, $^3G_5 \rightarrow {}^3H_6$ 2.2178 μm, $^3G_4 \rightarrow {}^3H_4$ 2.2437 μm, and $^3G_5 \rightarrow {}^3H_5$ 2.3485 μm due to [Fe III] (Sugar & Coliss 1985) are also clearly evident in our low-resolution spectrum of IRS 13. The ratio of the emission from the 2.3485 μm line to that of the 2.2178 μm line measures the extinction to the line-emitting region since both come from the same upper level. Assuming the Einstein A-values of Garstang (1957), the unreddened ratio should be 0.652; our measured ratio in the low-resolution spectrum is 0.88 ± 0.16, where we have estimated the uncertainty from the rms scatter in the nearby continuum. Assuming the extinction curve of Rieke & Lebofsky (1985) leads to a derived extinction of $A_K = 4 \pm 2$ mag, consistent with other estimates of the extinction to GC sources (i.e., Rieke et al. 1989; Wade et al. 1987). We adopt $A_K = 3$ mag as determined by these other, more accurate, methods.

The $^3G_5 \rightarrow {}^3H_6$ 2.2178 μm and $^3G_3 \rightarrow {}^3H_4$ 2.1457 μm [Fe III] lines were also detected in the high-resolution IRS 13 spectrum. These lines arise from closely spaced upper levels, so the ratio of the intensities is primarily density sensitive. Keenan et al. (1992) calculated collision strengths for Fe III and used the Einstein A-values of Garstang (1957) to produce relative level populations over a wide range of temperature and densities. The measured ratio of the two lines is 0.37 ± 0.1. Assuming $A_K = 3$, this suggests an unreddened value of 0.50 ± 0.1, which corresponds to $\log [n_e\,(\mathrm{cm}^{-3})] = 5.8 \pm 0.2$. Densities this high have also been estimated from [Fe II] lines in nearby regions by DePoy (1992).

At least one of the LMC Ofpe/WN9 class (HD 269858, not observed here) has been observed in transition to the spectrum like that of S Dor (Wolf et al. 1988). Our spectrum of HD 269582 shows an order of magnitude change in the He I 2.06 μm flux from that of MHH. Even with the potential uncertainties in our flux calibration, discussed above, the ratio of this line to Brγ has clearly changed from substantially greater than one in MHH to less than one in the present case. These two examples indicate an important area of investigation for the GC sources in the future: periodic observations showing spectral or continuum variations would provide strong links to the Ofpe/WN9 class.

3.3. *What Are They Not?*

The NIR spectra presented in Figure 1 can be used to eliminate several possibilities as to the nature of the GC He I

© American Astronomical Society • Provided by the NASA Astrophysics Data System

1995ApJ...441..603B

sources. Comparison to the spectra in Figure 3 indicates that the GC sources have NIR spectra much different from the prototype LBV, S Dor, or the galactic WN9 star, WR 108. The spectrum of WR 108 shows no evidence of He I 2.06 μm emission but does show emission at 1.700 and 2.11 μm (although, see the discussion above regarding the modeling of Crowther et al. 1994). Werner et al. (1990) present longer wavelength spectra of WR 108, IRS 16 NE, and AF which clearly show strong He II 3.09 μm emission in WR 108 and no 3.09 μm emission in AF or IRS 16 NE. The spectrum of S Dor is clearly distinct from the Ofpe/WN9 stars and GC sources in that it shows no He I emission. This is expected since the LBV maximum light phase (which S Dor is in) is expected to be a lower excitation one (BW). Ofpe/WN9 star spectra may be similar to LBV minimum light phase spectra. AG Car, a known LBV, has a K band spectrum with similar features as the LMC Ofpe/WN9 stars (MHH2) and was identified as Ofpe/WN9 at minimum by Stahl (1986) based on its optical spectrum. The well-known LBVs η Car (Allen, Jones, & Hyland 1985, and MHH2) and P Cyg (Libonate et al. 1995) also show similarities to the LMC Ofpe/WN9 K band spectra (MHH2).

The GC spectra are also significantly different from the NIR spectra of WN7–8 stars (Hillier 1985) which show quite strong P Cygni absorption in the 2.06 μm line, much weaker He I 2.06 μm relative to Brγ, and also He II emission in the H and K bands (Hillier's Figs. 2–8).

Earlier WR subtype, i.e. WC 5–9, can be ruled out by comparing the GC spectra to be observations of Eenens, Williams, & Wade (1991). All of these stars show strong C IV at 2.08 μm which dominates the He I emission at 2.06 μm.

The AF and AHH NW sources show distinct differences from the more normal O and B giant and supergiant K band spectra presented by Hanson & Conti (1994). Many of these spectra exhibit absorption features at 2.06 μm and 2.17 μm corresponding to He I and H I. Only one spectrum, that of the O7.5 III star HD 155806, shows strong emission at 2.06 μm relative to Brγ, but its He I 2.06 μm W_λ (7 Å) is much smaller than the AF, AHH NW, WR 122, WR 85a, and LMC stars. The W_λ for HD 155806 is similar to IRS 16 NW and SW. These two GC sources are much brighter than HD 155806, if individual sources. As Hanson & Conti point out, the emission from HD 155806 is presumably due to a disklike structure analogous to the Be star phenomenon. The large observed line widths (and no evidence of double peaked emission-line profiles) for a number of the GC sources are more naturally associated with wind outflow than disk emission.

3.4. *Mass-Loss Estimates for the GC Sources*

If we assume the Brγ emission in AF and the other GC sources arises in an optically thick outflow, as shown in § 3.1, then we can follow MMH2 in making simple estimates of the mass loss from each source. By using the results of Simon et al. (1983) for a constant velocity, completely ionized wind, we can determine the relative mass loss compared to AF for each of the sources from the Brγ integrated line fluxes. An estimate of the absolute mass loss can be obtained by taking the mass loss for AF as computed in the more detailed models of Najarro et al. (1994), which they give as $6.0–9.5 \times 10^{-5}\ M_\odot\ \mathrm{yr}^{-1}$. The estimate assumes each of the sources has similar He abundance, since the mass-loss rate for this model is proportional to the mean molecular weight (Krabbe et al. 1991). Assuming AF has the largest He abundance of the GC sources, based on the ratios of He I 2.06 μm and 2.11 μm to Brγ, then the mass-loss rates for the remaining GC sources may be overestimated. The recent model results presented for LMC Ofpe/WN9 stars by Crowther et al. (1994) indicate that the LMC stars may have a He/H abundance (by number) a factor of 3 less than AF. In addition, most of the other GC sources exhibit little or no He I 2.11 μm emission, except AHH NW (see Table 1). Note that the increased He I abundance for AF may be countered somewhat by the fact that He I (7–4) will be added to the Brγ line flux (Najarro et al. 1994). We find that the majority of the GC sources have somewhat smaller mass loss rates than AF, while the galactic and LMC stars fall in a wide range above and below the mass-loss rate for AF.

The values in Table 1 and range of model results for AF (Najarro et al. 1994) indicate a total mass-loss rate from all the He I sources at the GC of $\lesssim 6.0–9.5 \times 10^{-4}\ M_\odot\ \mathrm{yr}^{-1}$ (accounting for a total of twice the number of sources in the GC that we have observed, roughly the number of He I sources reported by Krabbe et a. 1991), in agreement with Krabbe et al. (1991). We note that these values are a factor of 3–5 less than that required by Gatley et al. (1984, $3 \times 10^{-3}\ M_\odot\ \mathrm{yr}^{-1}$) to collisionally excite the H_2 emission observed at the edge of the 2 pc molecular ring. The observed cometary tail of the red supergiant IRS 7 has been interpreted by Serabyn, Lacy, & Achtermann (1991) and Yusef-Zadeh & Melia (1992) as arising from the impact of a wind from the IRS 16 vicinity on IRS 7. Both Serabyn et al. and Yusef-Zadeh & Melia argue for a wind mechanism instead of a drag force due to the motion of IRS 7 through the GC interstellar medium, although neither of their results rule out the drag force scenario. Yusef-Zadeh & Melia fit the observed bow shock structure to simple models which result in a best-fit required mass loss from the vicinity of IRS 16 of about $1.5 \times 10^{-3}\ M_\odot\ \mathrm{yr}^{-1}$. They cannot rule out somewhat lower values of the required mass loss, which would be more consistent with the values presented here. Serabyn et al. compute models of the tail kinematics for various values of the ratio of the force on the tail due to an external wind, relative to the force of gravity due to the GC mass distribution. This parameter includes, but does not necessarily constrain, the mass-loss rate since it is also affected by the GC mass distribution and tail density; the implied mass-loss rate in the wind could be consistent with the values reported here.

3.5. *The H-R Diagram*

The ultimate goal of the analysis of the NIR spectra of the GC sources is to use the resulting spectral type information to assess the overall impact these objects have on the GC environment. Placing the GC sources in the H-R diagram would result in firm estimates of the total ionizing flux and mass loss expected. The above results clearly indicate that we have not reached this point. However, the emission-line spectra of the GC sources are at least suggestive that some of these objects are similar to very massive evolved stars. Therefore, we have used published data for WR, Ofpe/WN9, and LBV stars to compute K band bolometric corrections (BC_K) as a function of stellar effective temperature (Fig. 5) which we apply to the GC sources. The resulting H-R diagram is shown in Figure 6, where the GC sources are represented as line segments corresponding to different BC_K's. The vertical error bar (± 0.71 mag) is an estimate of the uncertainty in the bolometric correction, estimated by the scatter in the best-fit linear relation shown in Figure 5, added in quadrature to a ± 0.5 mag uncertainty in the adopted reddening.

© American Astronomical Society • Provided by the NASA Astrophysics Data System

1995ApJ...441..603B

The BC_K's were determined from the photometry and stellar parameters given in Table 4. Reddening values were determined from the published $E(B-V)$ or A_V values and by assuming $R = 3.1$ and the interstellar reddening curve of Rieke & Lebofsky (1985). The BC_K's were then fitted to a line using a least-squares analysis. The data and fit are shown in Figure 5. We take the average residual (0.5 mag) as an estimate in the uncertainty of the BC_K at any given $T_{\rm eff}$. The BC_K relationship has a similar slope but is approximately 1 mag fainter than the same relation derived for a blackbody.

The GC source photometry are taken from the references given in Table 4. In the case of IRS 13 and IRS 1 W, the K magnitudes were taken from Simon et al. (1990). The results of Simon et al. 1990) are based on lunar occultations of the GC and indicate that IRS 1 W and 13 are composed of two dominant sources each. For purposes of including them in the H-R diagram, we will take a K mag corresponding to the brighter of the two sources. The distance and reddening to the GC are taken as 8 kpc (Reid 1989) are $A_K = 3.0$ mag (Wade et al. 1987), respectively.

The NIR spectra of the GC sources indicate that none of them is consistent with WN8 or earlier type massive stars. The GC tracks in Figure 6 then suggest that none of the bright blue sources in the GC is as hot as the limiting $T_{\rm eff}$ ($\lesssim$35,000 K) for sources which ionize the diffuse gas in the central few pc (Serabyn & Lacy 1985). The similarity of the NIR spectra of the GC sources to several of the sources in Figure 3, but not the hotter WN7–8 stars suggests as limiting $T_{\rm eff}$ for the He I emission-line stars of $\approx$30,000 K. If we assume all the GC sources are at their maximum $M_{\rm bol}$, then they would produce $\approx 3.8 \times 10^{50}$ s^{-1} Lyman continuum photons (accounting for twice the number of He I sources that we have observed, Krabbe et al. 1991, and including IRS 1 W). Here we have used the flux of ionizing photons from Panagia (1973), assuming $T_{\rm eff} \approx$ 30,000 K and a stellar radius appropriate to the $M_{\rm bol}$ give in Table 4. This is just sufficient to account for the required H I ionizing flux in the GC (Serabyn & Lacy 1985; Mezger & Wink 1986).

It is likely that some of the GC He I sources are actually cooler and less luminous than the maximum case shown in Figure 6. Krabbe et al. 1991) report that supergiant stars of $T_{\rm eff} \approx$ 31,000 K would produce 0.06 He I ionizing photons for each Lyman continuum photon. In this case, the total number of He I ionizing photons produced by the GC sources (using the maximum BC_K for each source) would exceed the number predicted by Krabbe et al. (1991) from analysis of the observed He I emission in the central few pc. The models of Najarro et al. (1994) estimate that AF has a $T_{\rm eff} \approx$ 20,000 K and that AF produces $\lesssim 10^{48}$ s^{-1} H I ionizing photons and $\lesssim 10^{38}$ s^{-1} He I ionizing photons. This $T_{\rm eff}$ (based on $M_{\rm bol}$ and radius at the base of the wind) is significantly less than the $T_{\rm eff}$ ($\approx$29,000 K) derived for the LMC Ofpe/WN9 stars modeled by Crowther et al. (1994; they call $T_{\rm eff}$, as defined here, T_*). The Najarro et al. results are shown by the box labeled N94 in Figure 6 and are consistent, within the estimated uncertainty, with the BC_K derived here.

The minimum $T_{\rm eff}$ used in determining the BC_K for the GC sources corresponds to $\approx$14,000 K. This is the value for HR Car and represent an approximate lower limit to the $T_{\rm eff}$ which can excite the observed He I emission. The K band spectrum of HR Car (MHH2) has essentially no He I 2.06 μm emission.

The H-R diagram suggests that all eight GC sources observed here may be massive post–main-sequence stars with initial masses between $\approx$15 and 100 $M_\odot$. Several of these sources may be near the Humphreys-Davidson limit (however, note that the K band spectrum of IRS 1 W is not similar to the

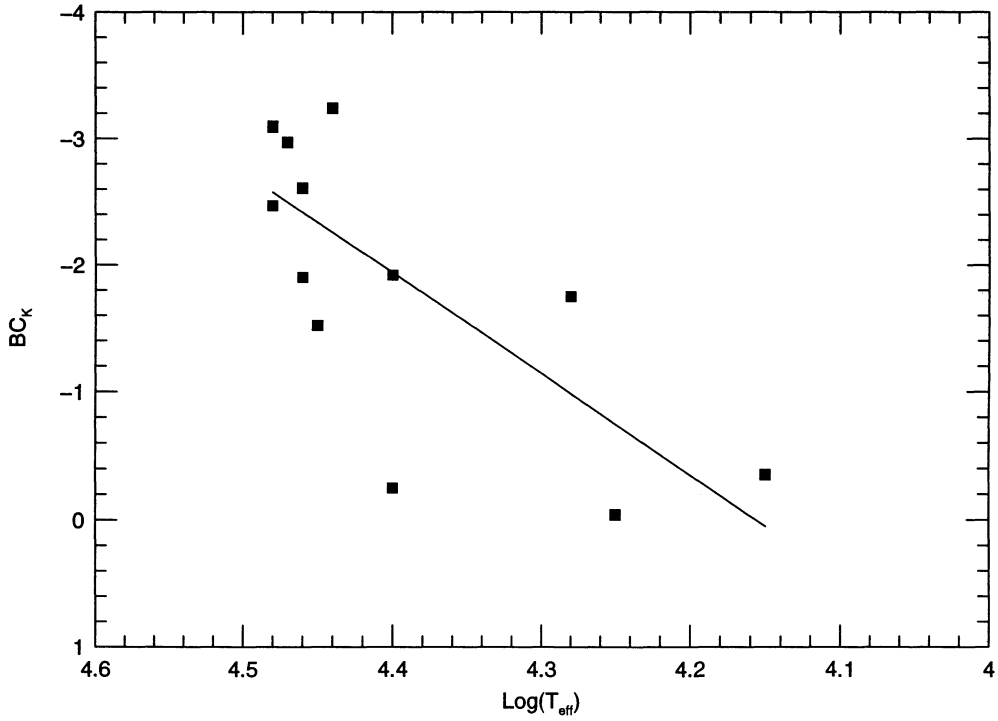

FIG. 5.—Derived K band bolometric corrections (*filled squares*) for the early-type mass-losing stars listed in Table 4. The solid line is the best-fit linear relation between the bolometric correction and effective temperature.

© American Astronomical Society • Provided by the NASA Astrophysics Data System

1995ApJ...441..603B

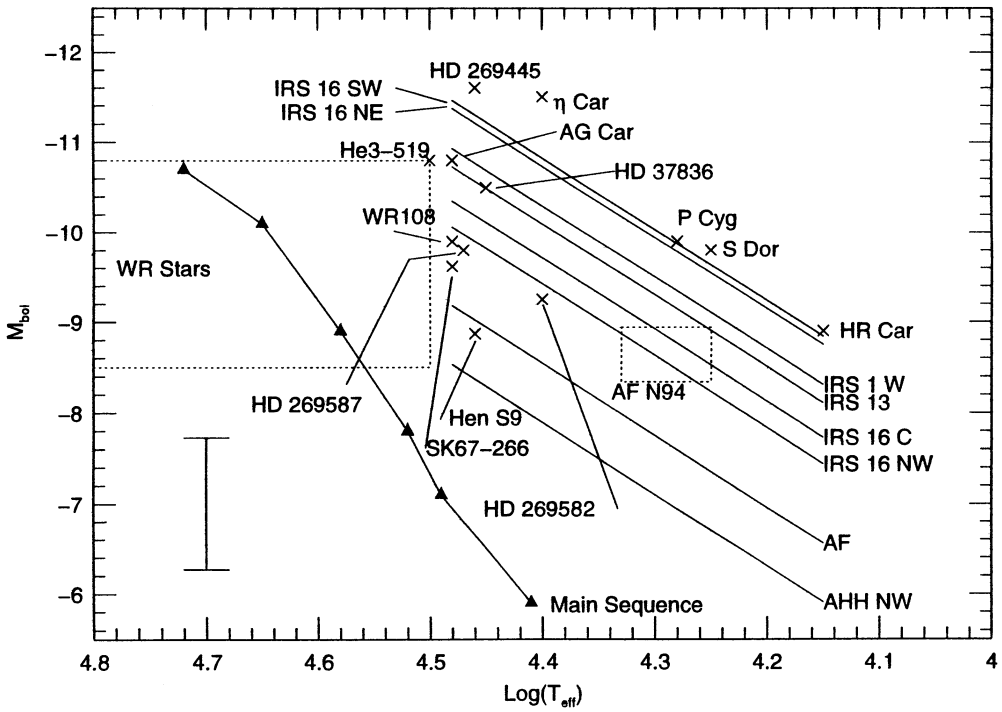

FIG. 6.—H-R diagram for the GC sources and early-type mass-losing stars. The GC sources are shown as solid lines using the bolometric correction vs. effective temperature relationship shown in Fig. 5. Data for the individual comparison sources (*crosses*) are taken from the references given in Table 4. The larger box (*dashed lines*) labeled "WR Stars" is reproduced from Humphreys & Davidson (1994). The smaller box (*dashed lines*) labeled "AF N94" depicts the model results of Najarro et al. (1994) for the AF source. The error bar shown is for the GC sources and corresponds to a ± 0.71 mag uncertainty in M_{bol} estimated from the residuals in the fit of Fig. 5 added in quadrature to an assumed ± 0.5 mag uncertainty in the adopted reddening. The main sequence (Schmidt-Kaler 1982) is shown for comparison (*filled triangles*).

spectra of the galactic and LMC comparison stars) while others have bolometric luminosities which overlap with those of late O and B supergiants.

4. CONCLUSIONS

Direct comparison of the GC He I emission-line source, AF, with representatives of the Ofpe/WN9 class shows that its NIR spectrum is morphologically similar to the spectra from these early-type mass-losing stars. However, we find significant evidence that the AF and AHH NW sources and galactic Ofpe/WN9 stars WR 122 and WR 85a may have substantial differences in the physical conditions in their mass-losing envelopes relative to the LMC stars. They show an order of magnitude larger equivalent width in the He I 2.06 μm line than the LMC stars. In addition, we find larger velocity widths in the He I lines in the AF and other GC sources (observed widths up to 1200 km s^{-1}) than in any of the galactic or LMC Ofpe/WN9 stars, which are unresolved (or marginally resolved) at our resolution ($\lesssim$565 km s^{-1} at 2.06 μm and 513 km s^{-1} at 1.70 μm). The observations of Crowther et al. (1994) are consistent with our finding that higher velocity outflows occur in the GC sources.

We point out that the models of Crowther et al. (1994) for a number of LMC Ofpe/WN9 stars result in significant differences from the predictions for AF of Najarro et al. (1994) for several of the derived stellar parameters. The He abundance predicted by Najarro et al. for AF is much larger than the values derived by Crowther et al. for the LMC stars: He/H by number of 1.3 ± 0.3 compared to 0.3 ± 0.1. Evolutionary models for massive stars (Maeder 1990) predict that the surface abundance of He relative to H will change significantly over short evolutionary times, so the observed difference in He/H may not be significant. The temperature (based on M_{bol} and radius at the base of the atmosphere) is higher for the LMC stars modeled by Crowther et al. compared to the Najarro et al. result for AF.

While in general agreement with previous work, the GC spectra presented here include several new important aspects. The long-slit capability and spatial scale of OSIRIS allow us to determine the nearby background contribution to the GC sources. This is essential in the eliminating emission from diffuse gas and in estimating the true underlying continuum for the GC sources. We find that the He I source IRS 1 W has no emission at 2.06 μm after background subtraction, consistent with it being an H II region with an embedded source which has no compact He I emission.

Our spectra also greatly expand the wavelength coverage of the GC He I sources including the He I 2.113 μm region. We find that the He I emission near 2.06 and 2.11 μm may extend farther to the red than previously found for some sources. IRS 13 is the most prominent example of this type. While we cannot rule out that this emission is due to unidentified, unresolved lines, our high-resolution spectrum of IRS 13 suggests the He I 2.06 and 2.11 μm lines have continuous asymmetric emission profiles extending to the red of line center.

Finally, we point out that a large range of broad-band and spectroscopic measurements should be used in modeling the GC sources. The NIR photometry and spectra (WR 122 and WR 85a in Fig. 2 are extreme examples) indicate that we should expect an excess of continuum emission due to free-free and/or dust emission to be present in the GC sources if they are similar to the Ofpe/WN9 class. This is especially important

© American Astronomical Society • Provided by the NASA Astrophysics Data System

1995ApJ...441..603B

in the GC where large observed colors are often attributed entirely to interstellar extinction.

The broad-band fluxes and spectra of the GC sources should also be observed for evidence of variability. Several of the LMC stars are known variables and one of them, HD 269582, showed a large variation in the He I 2.06 μm line in the present work, relative to the spectrum presented by MHH.

This work was supported by the NSF grants AST 90-16112, AST 91-15236 and AST 92-18449. We thank the CTIO staff for their excellent assistance at the telescope, especially night assistants Hernan Tirado and Partricio Ugarte. We also thank Richard Pogge of OSU for use of the spectral line analysis program LINER.

REFERENCES

Abbott, D. C. 1982, ApJ, 259, 282
Allen, D. A. 1973, MNRAS, 161, 145
Allen, D. A., & Glass, I. S. 1974, MNRAS, 167, 337
Allen, D. A., Hyland, A. R., & Hillier, D. J. 1990, MNRAS, 244, 706
Allen, D. A., Jones, T. J., & Hyland, A. R. 1985, ApJ, 291, 280
Bernat, A. P., & Lambert, D. L. 1978, PASP, 90, 520
Bohannan, B., & Walborn, N. R. 1989, PASP, 101, 520 (BW)
Brockelhurst, M. 1972, MNRAS, 157, 211
Crowther, P. A., Hillier, D. J., & Smith, L. J. 1994, A&A, in press
Davidson, K., Humphreys, R. M., Hajian, A., & Terzian, Y. 1993, ApJ, 411, 336
DePoy, D. L. 1992, ApJ, 398, 512
DePoy, D. L., & Sharp, N. A. 1991, AJ, 101, 1324
DePoy, D. L., Atwood, B., Byard, P., Frogel, J. A., & O'Brien, T. 1993, in SPIE1946, "Infrared Detectors and Instrumentation," p. 667
DePoy, D. L., & Shields, J. C. 1994, ApJ, 422, 187
Dufour, R. J. 1986, PASP, 98, 1025
Eckart, A., Genzel, R., Hofmann, B., Sams, B. J., & Tacconi-Garman, L. E. 1993, ApJ, 407, L77
Eenens, P. R. J., Williams, P. M., & Wade, R. 1991, MNRAS, 252, 300
Forrest, W. J., Shure, M. A., Pipher, J. L., & Woodward, C. E. 1987, in The Galactic Center, ed. D. C. Backer (New York: AIP)
Garstang, R. H. 1957, MNRAS, 117, 393
Gately, I., Jones, T. J., Hyland, A. R., Beattie, D. H., & Lee, T. J. 1984, MNRAS, 210, 565
Genzel, R., Hollenbach, D., & Townes, C. H. 1994, Rep. Prog. Phys., in press
Genzel, R., & Townes, C. H. 1987, ARA&A, 25, 377
Hanson, M. M., & Conti, P. S. 1994, ApJ, 423, L139
Hillier, D. J. 1984, ApJ, 280, 744
———. 1985, AJ, 90, 1514
———. 1991, A&A, 247, 455
Hummer, D. G., & Storey, P. J. 1987, MNRAS, 224, 801
Humphreys, R. M., Lamers, H. J. G. L., Hoekzema, N., & Cassatella, A. 1989, A&A, 218, L17
Humphreys, R. M., & Davidson, K. 1994, PASP, submitted
Hutchings, J. B. 1980, ApJ, 235, 418
Keenan, F. P., Berrington, K. A., Burke, P. G., Zeippen, C. J., Le Dourneuf, M., & Clegg, R. E. S. 1992, ApJ, 384, 385
Krabbe, A., Genzel, R., Drapatz, S., & Rotaciuc, V. 1991, ApJ, 382, L19
Kurucz, R. L. 1979, ApJS, 40, 1
Lacy, J. H., Townes, C. H., Geballe, T. R., & Hollenbach, D. J. 1980, ApJ, 241, 132
Lamers, H. J. G. L., de Groot, M., & Cassetella, A. 1983, A&A, 128, 299
Lebofsky, M. J., Rieke, G. H., & Tokunaga, A. T. 1982, ApJ, 263, 736
Leitherer, C., Appenzeller, I., Klare, G., Lamers, H. J. G. L. M., Stahl, O., Waters, L. B. F. M., & Wolf, B. 1985, A&A, 153, 168
Libonate, S., Pipher, J. L., Forrest, W. J., & Ashby, M. L. N. 1995, ApJ, 439, 202
Lutz, D., Krabbe, A., & Genzel, R. 1993, ApJ, 418, 244
Maeder, A. 1990, A&AS, 84, 139
McGregor, P. J., Hillier, D. J., & Hyland, A. R. 1988, ApJ, 334, 639 (MHH)
McGregor, P. J., Hyland, A. R., & Hillier, D. J. 1988, ApJ, 324, 1071 (MHH2)
Mezger, P. G., & Wink, J. E. 1986, A&A, 157, 252
Morris, M. 1993, ApJ, 408, 496
Najarro, F., Hillier, D. J., Kudritzki, R. P., Krabbe, A., Genzel, R., Lutz, D., Drapatz, S., & Geballe, T. R. 1994, A&A, in press
Oliva, E., & Origlia, L. 1992, A&A, 254, 466
Panagia, N. 1973, AJ, 78, 929
Phinney, E. S. 1989, IAU Symp. 136, The Center of the Galaxy, ed. M. Morris (Dordrecht: Kluwer) 543
Reid, M. J. 1989, in IAU Symp. 136, The Center of the Galaxy, ed. M. Morris (Dordrecht: Kluwer) 37
Rieke, G. H., & Lebosfsky, M. J. 1982, in The Galactic Center, ed. G. R. Riegler & R. D. Blandford (New York: AIP), 194
———. 1985, ApJ, 288, 618
Rieke, G. H., Rieke, M. J., & Paul, A. E. 1989, ApJ, 336, 752
Schmidt-Kaler, T. 1982, in Landoldt-Bornstein, Numerical Data and Functional Relationships in Science and Technology, Vol. 2 (Berlin: Springer) 453
Serabyn, E., & Lacy, J. H. 1985, ApJ, 293, 445
Serabyn, E., Lacy, J. H., & Achtermann, J. M. 1991, ApJ, 378, 557
Shields, J. C. 1993, ApJ, 419, 181
Shields, J. C., & Ferland, G. 1994, ApJ, 430, 236
Simon, M., Chen, W. P., Forrest, W. J., Garnett, J. D., Longmore, A. J., Gauer, T., & Dixon, R. I. 1990, ApJ, 360, 95
Simon, M., Felli, M., Cassar, L., Fischer, J., & Massi, M. 1983, ApJ, 266, 623
Simons, D. A., Hodapp, K. W., & Becklin, E. E. 1990, ApJ, 360, 106
Stahl, O. 1986, A&A, 164, 321
Stahl, O., Wolf, B., de Groot, M., & Leitherer, C. 1985, A&AS, 61, 237
Sugar, J., & Corliss, C. 1985, J. Phys. Chem. Ref. Data, 14, Suppl. 2
Tamblyn, P., & Rieke, G. H. 1993, ApJ, 414, 573
van der Hucht, K. A., Hidayat, B., Admiranto, A. G., Supelli, K. R., & Doom, C. 1988, A&A, 199, 217
van Genderen, A. M., Robijn, F. H. A., van Esch, B. P. M., & Lamers, H. J. G. L. 1991, A&A, 246, 407
Wade, R., Geballe, T. R., Krisciunas, K., Gatley, I., & Bird, M. C. 1987, ApJ, 320, 570
Walborn, N. R. 1977, ApJ, 215, 53
Werner, M. W., Stauffer, J. R., & Becklin, E. E. 1990, in Evolution of the Universe of Galaxies, ed. R. Kron (PASP Conf. Ser., Vol 10), 167
Wiese, W. L., Smith, M. W., & Glennon, M. 1966, NSRDS-NBS, No. 4
Williams, P. M., van der Hucht, K. A., & Thé, P. S. 1987, A&A, 182, 91
Wolf, B., Stahl, O., Smolinski, J., & Cassetella, A. 1988, A&AS, 74, 239
Yusef-Zadeh, F., & Melia, F. 1992, ApJ, 385, L41

© American Astronomical Society • Provided by the NASA Astrophysics Data System